Separation Science and Technology
Publication details, including instructions for authors and subscription information:
http://www.informaworld.com/smpp/title~content=t713708471

Density Separation of Solids in Ferrofluids with Magnetic Grids

Homer Fay[a]; Jean M. Quets[b]
[a] Union Carbide Corporation Linde Division, Tonawanda Laboratory, Tonawanda, NY [b] Union Carbide Corporation Linde Division, Speedway Laboratory, Speedway, IN

To cite this Article Fay, Homer and Quets, Jean M.(1980) 'Density Separation of Solids in Ferrofluids with Magnetic Grids', Separation Science and Technology, 15: 3, 339 — 369
To link to this Article: DOI: 10.1080/01496398008068487
URL: http://dx.doi.org/10.1080/01496398008068487

SEPARATION SCIENCE AND TECHNOLOGY, 15(3), pp. 339-369, 1980

DENSITY SEPARATION OF SOLIDS IN FERROFLUIDS WITH MAGNETIC GRIDS

Homer Fay
Union Carbide Corporation
Linde Division
Tonawanda Laboratory
Tonawanda, NY 14150

and Jean M. Quets
Union Carbide Corporation
Linde Division
Speedway Laboratory
Speedway, IN 46224

ABSTRACT

Nonmagnetic solids in a superparamagnetic ferrofluid are subjected to body forces proportional to the intensity of magnetization of the fluid and the gradient of the magnetic field. An apparent density of the fluid can be defined from the force equations, and since the apparent density can be much larger than the true density, it is possible to levitate or float dense objects. Mixtures of solids with a density greater than the apparent density sink while lower density solids float.

In practice it is difficult to create a uniform gradient over a large volume and "single gap" magnetic separators require very large magnets or have a limited throughput. To overcome that problem, "multiple gap" magnetic grids have been designed. Such grids consist of planar arrays of parallel bars of alternating polarity, driven by permanent magnets. When immersed in ferrofluid, magnetic grids create nonuniform field gradients and apparent densities in the fluid. However, both analysis and experimental measurements show that the grid acts as a barrier to particles below a critical density, while permitting more dense particles

to fall through the grid. Thus, a magnetic grid filter can be used as a high throughput binary separator of solids according to their densities. Such filters can be cascaded for more complex separations.

Several magnetic grid filters have been designed, built, and tested. Magnetic measurements qualitatively agree with the theoretical predictions. Experiments with synthetic mixtures have demonstrated that good binary separations can be made.

INTRODUCTION

The unusual properties of "ferrofluids" have been intensively studied in recent years and were reviewed at an international workshop in 1977 (1). Such fluids are superparamagnetic and are strongly influenced by magnetic fields. Rosensweig (2-4) and others (5-7) have developed processes for levitating dense nonmagnetic objects in ferrofluids, based on the attraction of the fluid by the field. A field gradient can be established in the ferrofluid in the gap of a large magnet, so that there will be an upward buoyant force on the object of sufficient magnitude to oppose the downward force of gravity. In this way one can levitate the densest materials on earth.

Since the levitation depends on the density, it is possible to use ferrofluids to separate solid objects of different densities. Density separation processes based on ferrofluids have been developed by the Avco Corporation (2-5, 8) and by the U. S. Bureau of Mines (6, 7). The ferrofluid and the objects to be separated are contained within or pass through the gap of a large electromagnet. The pole pieces of the magnet are usually shaped to create a nearly uniform field gradient over a substantial volume. Although such processes are workable, they require expensive energy-consuming magnets. The material throughput is limited because all of the material to be separated must pass through the relatively small gap region. It is difficult to "scale-up" the process without increasing the size or number of large magnets.

In this paper, we describe a different way to create the required field gradients by use of "magnetic grids". There are arrays of parallel poles of alternating polarity that can be completely immersed in the ferrofluid. Analysis and experiments both show that the nonuniform field gradients near such structures can act as a barrier to low density particles while permitting high density particles to fall through the grid. The design of magnetic grids and their use in practical binary density separation processes will be described.

Ferrofluid Properties

Ferrofluids are complex colloidal suspensions of ferromagnetic particles in a liquid vehicle. In our laboratory we have developed methods for making multi-liter quantities of ferrofluids of magnetite in kerosene, using a variation of the peptization process of Reimers (9). These fluids are stable and of sufficient strength for use in magnetic separation processes. Processes for reconcentrating diluted ferrofluids have also been developed in our laboratory.

Ferrofluids have many fascinating characteristics, but the property of most interest in density separations is the magnetization induced in the fluid by a magnetic field. The shape of the magnetization curve is shown schematically in Figure 1, where we plot the intensity of magnetization I as a function of the applied field H (10). After an initial linear region, the intensity approaches a saturation value, I_s, for relatively low values of the applied field. The curve is single-valued and exhibits no hysteresis. This form of magnetization is characteristic of superparamagnets and the curve should ideally follow the Langevin function. Real fluids have a distribution of particle sizes and may deviate appreciably from the ideal. The magnetization curve of a ferrofluid can be directly displayed on an oscilloscope with a loop-tracer circuit previously described (11).

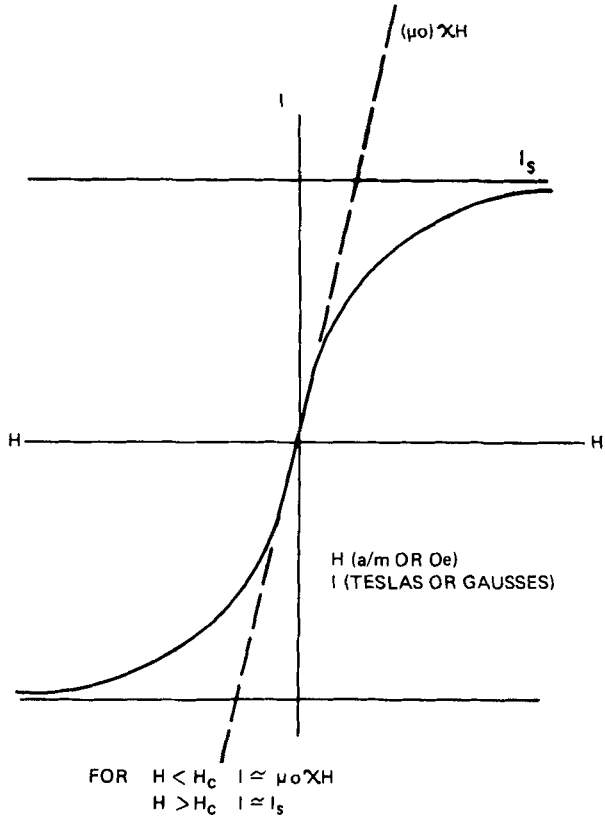

FIGURE 1 Magnetization curve for ferrofluid.

A typical kerosene based ferrofluid will saturate in a field of ca 10^3 Am^{-1} and have an intensity of magnetization of 0.02-0.04 T. The true density will be near that of water (10^3 kg m^{-3}) and the viscosity ca 4 x 10^{-3} kg m^{-1} s^{-1}. In the analyses given below, we shall usually assume that the field exceeds the critical value and that the magnetization is saturated. The fluid strength is taken to be the saturation magnetization I_s.

Forces in Ferrofluids

A rigid solid object immersed in a ferrofluid in a magnetic field is subjected to several forces. The gravitational force F_g, acting downward on the body is

$$\vec{F}_g = (m_o - m_f)\,\vec{g} = V_o\,(\rho_o - \rho_f)\,\vec{g} \qquad (1)$$

where m_o and m_f are the masses of the object and the displaced fluid, V_o is the volume of the object, ρ_o and ρ_f are the densities of the object and the fluid, and $\vec{g}$ is the gravitational acceleration. Due to the presence of the ferrofluid, a magnetic force $\vec{F}_m$ also acts on the object. This force is

$$\vec{F}_m = V_o\,(I_o - I_f)\,\vec{\nabla H} \qquad (2)$$

where I_o and I_f are the intensities of magnetization of the object and the ferrofluid, and $\vec{\nabla H}$ is the gradient of the magnetic field. This force acts in the direction of the gradient. These are the only relevant static forces, but additional forces of hydrodynamic resistance appear when the object moves through the fluid.

If the vector sum of the static forces is zero, the object will be stationary. By defining the vertical positive direction as upward, and noting that $\vec{g}$ is directed downward, equilibrium is obtained when

$$(I_o - I_f)\,\vec{\nabla H} = (\rho_o - \rho_f)\,\vec{g} \qquad (3)$$

For Eq 3 to be obeyed, the gradient must be vertical and $\vec{\nabla H} = \nabla H_z = dH/dz$. The particular value of ρ_o that satisfies Eq 3 may be defined as the "apparent density" of the ferrofluid. In the usual case where the object is nonmagnetic, the apparent density is given by

$$\rho_a = \rho_f - I_f\,\nabla H_z/g \qquad (4)$$

An object of density $\rho_o > \rho_a$ will tend to sink in the fluid, whereas an object of density $\rho_o < \rho_a$ will tend to float.

The concept of apparent density can be extended to regions where the gradient has a horizontal component but only the vertical component is used in Eq 4.

Analysis of Simple Grids

A magnetic grid is a planar array of parallel bars of alternating magnetic polarity. The construction of real magnetic grids is described in a later section. The magnetic field around

real grids is complex, but can be approximated by considering ideal grids, where the poles are represented by small semi-infinite cylinders or wires.

The problem of determining the spatial distribution of the field near an array of cylindric magnetic poles is analogous to finding the field near current-carrying wires, which may be calculated by Ampere's law. At a given point in space, the field produced by each wire is found and the vector sum gives the total field. The method yields analytic solutions for simple cases and machine computations may be used for more complex arrays. The gradient of the magnitude of the field may be found by differentiation.

For the trivial case of a single wire carrying a current J, the field at a distance r is $H = J/2\pi r$. The gradient is $\nabla H = -J/2\pi r^2$, directed radially. If such a single wire or pole were immersed in ferrofluid, the gradient would act to repel nonmagnetic objects from the wire.

The next simplest case is two wires separated by a distance 2a, carrying equal but oppositely directed currents, J. The magnitude of the field is found to be

$$H = \frac{J}{\pi a}\left[\frac{1}{\left[(y+1)^2+z^2\right]\left[(y-1)^2+z^2\right]}\right] = \frac{J}{\pi a}\,h \qquad (5)$$

where y and z are the distances from the center between wires, in units of a. A map of the function h is shown in Figure 2. High values of H occur near the wires and low values far away, with a saddle point at the origin. The magnitude of the gradient may be expressed as

$$\nabla H = \frac{-2J}{\pi a^2}\left[\frac{(y^2+z^2)^{1/2}}{\left[(1+y)^2+z^2\right]\left[(1-y)^2+z^2\right]}\right] = \frac{-2J}{\pi a^2}\,f \qquad (6)$$

A map of the function f is shown in Figure 3. The gradient vanishes at the origin and at infinity. The vertical component of the gradient vanishes at z = 0. High values occur near the wires where the contours circle each wire. Lower valued contours map around both wires. There is a critical value (f=.325) which

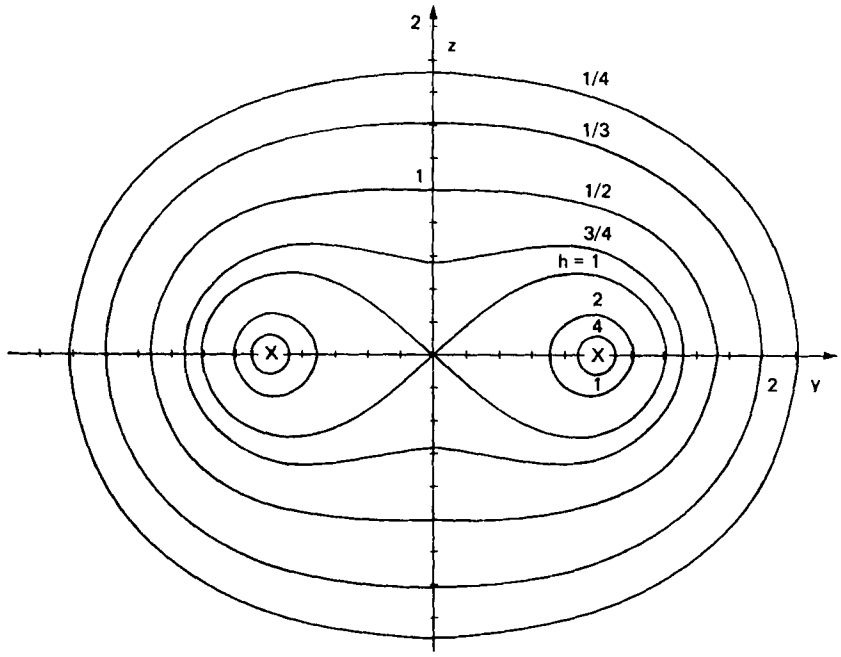

FIGURE 2 Map of the magnetic field intensity around two conductors. Dimensions are relative to a, where 2a is the distance between wires.

separates the two regimes. This is the least of the high values of f encountered on any path between the wires. If the wire pair were immersed in ferrofluid only objects that could surmount this gradient could pass between the wires.

Complete analytic solutions can be derived for larger arrays, but they are cumbersome and machine calculations are preferred. However, there are special positions where the analysis is greatly simplified by symmetry. The vertical central plane dividing an array of wires in half is such a special position. For an even number of wires and an odd number of gaps, the problem degenerates to computing the cumulative effect of pairs of wires spaced at progressively greater distances. The field and field gradient are given by oscillating series of term

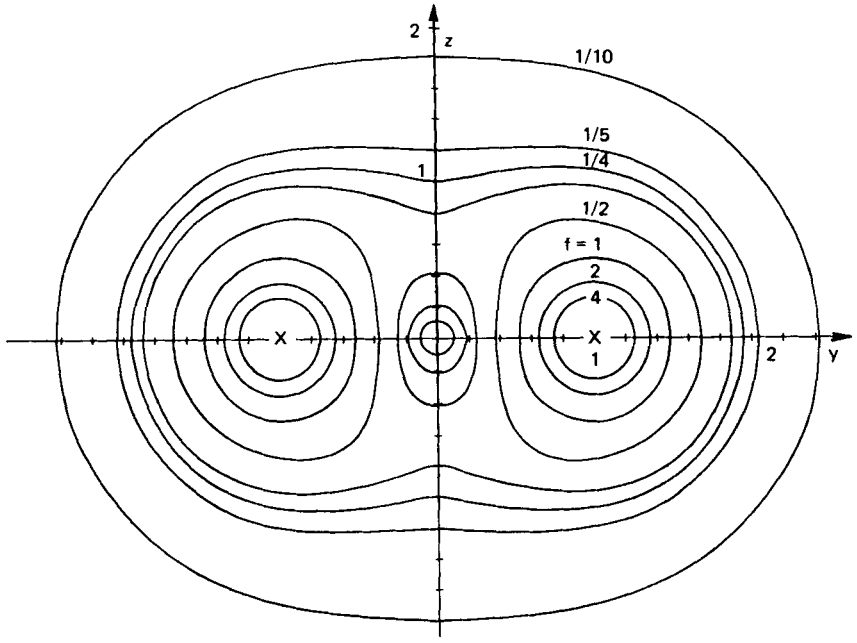

FIGURE 3 Map of the magnitude of the field gradient around two conductors. Dimensions are the same as Figure 2.

$$H = \frac{J}{\pi a}\left[\frac{1}{1+z^2} - \frac{3}{9+z^2} + \frac{5}{25+z^2} \text{ --- } \pm \frac{n}{n^2+z^2}\right] \quad (7)$$

$$= H_s\, h_n \quad (7a)$$

$$\nabla H = \frac{-2J}{\pi a^2}\left[\frac{z}{(1+z^2)^2} - \frac{3z}{(9+z^2)^2} - \frac{5z}{(25+z^2)^2} \text{ --- } \pm \frac{nz}{(n^2+z^2)^2}\right] \quad (8)$$

$$= (-2H_s/a)\, f_n \quad (8a)$$

where z is the vertical distance above the grid in units of a. The gradient is vertical on this plane; there is no horizontal component. While the field function h_n is symmetric about the grid, the gradient function f_n depends on the sign of z and will change from upward to downward in passing through the plane of the grid. The functions h_n and f_n are plotted in Figure 4 and Figure 5. The h_n function is

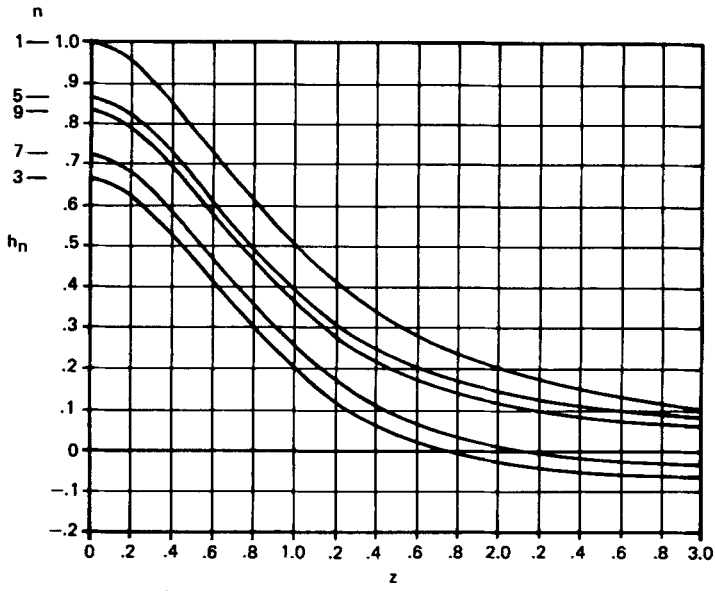

FIGURE 4 Plot of the field function h_n for an array of n+1 conductors and n gaps. The distance z is in units of a, the half-spacing of the conductors.

displaced as the number of gaps n increases, due to the oscillating series, and can even have negative values. The f_n function is less effected by the number of wires. The position of the maximum is essentially unchanged and the peak value is nearly constant. This is important in the separation processes to be described, because it means that the local forces do not depend appreciably on the number of wires or poles.

For an infinite array of wires, the value of h_n at the origin approaches $\pi/4$. It is convenient to define the maximum value of H for a single pair of wires as H_s, the standard central field, which corresponds to $h_n = 1$. For an infinite array the central field H_o will be $(\pi/4)H_s$. The critical gradient corresponds to the maximum value of f_n. It occurs at a level close to $z = 1/\sqrt{3} = .58$, which is the exact value for a single gap. The value of f_n at this height varies with n according to the table.

n	f_n (at $z=1/\sqrt{3}$)
1	.325
3	.305
5	.309
7	.308
.	.
∞	.30823

The convergence is rapid and for all practical purposes, that peak value is constant and equal to .31. The insensitivity of f_n to the value n indicates that each gap of a large grid acts approximately the same.

Machine calculations have been used to find the magnetic field, the magnitude of the field, the gradient of the field, the magnitude

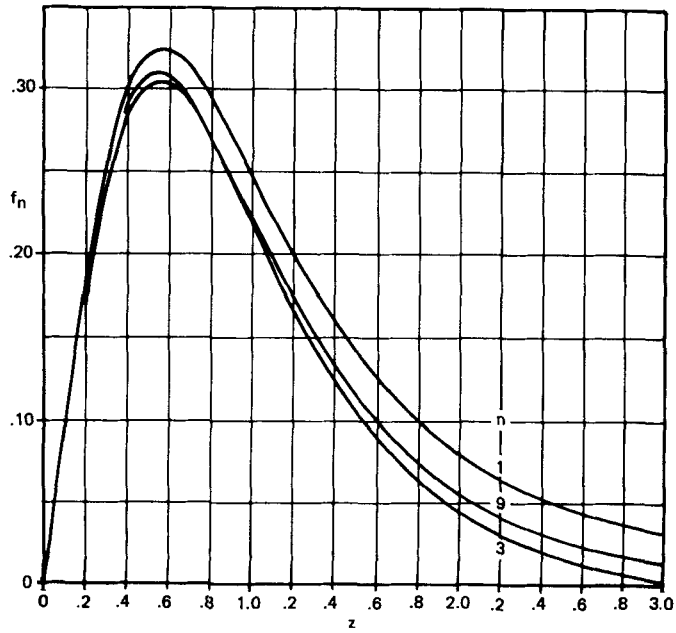

FIGURE 5 Plot of the gradient function f_n for an array of n+1 conductor and n gaps. The distance z is the same as in Figure 4. Note that the peak positions and peak heights are nearly identical.

of the gradient and the horizontal and vertical components of the gradient around magnetic grid structures. The vertical component of the gradient determines the apparent density according to Eq 4. A contour map of the vertical component of the gradient in the region above five wires of a large array is shown in Figure 6. Low values map as wavy sheets over the grid; high values map as lobes over the wires. A critical value separates the two regimes. The critical contour has saddle points on the vertical planes midway between the wires. These points represent the highest value on these planes and are called the critical points. A similar map could be drawn below the plane of the wires, but these forces are directed downward and cannot produce levitation.

Various computational methods have been used to determine the magnetic fields near shaped poles of finite dimensions. Corners and sharp edges on the poles create local perturbations of the fields but, in general, the pole shape has a relatively small effect on the contour maps. Rounded poles produce vertical forces quite

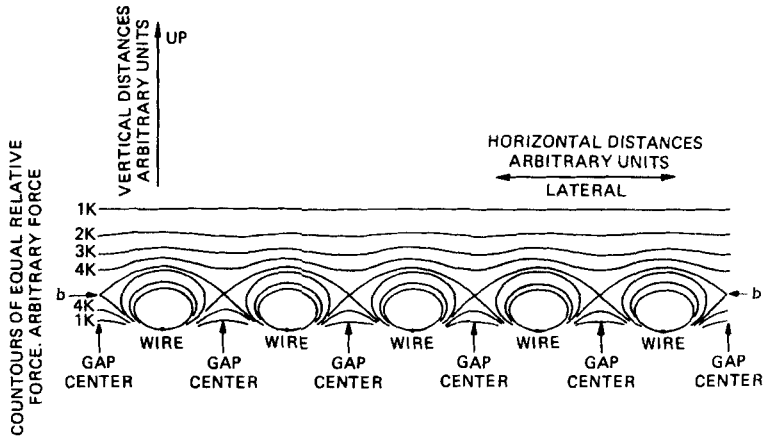

FIGURE 6 Contour map of the vertical forces near five wires of a large array. The critical points occur at b and similar points.

similar to Figure 6, but the size of the pole must be accommodated.

Density Separation in Nonuniform Gradients

An ordinary fluid of density ρ_f may be used to separate solids. Objects more dense than ρ_f sink while objects less dense than ρ_f float. For a ferrofluid the separation depends on the apparent density ρ_a, which depends on the vertical component of the gradient by Eq 4. The density of an ordinary fluid is uniform over its volume. It is natural to want to make ρ_a uniform over an appreciable volume to make it analogous to normal fluids. This requires that the vertical component of the gradient be uniform. Specially shaped pole pieces have been used to create regions where the gradient is nearly uniform (8). This is unnecessary. Density separations can be performed in the nonuniform gradients produced by magnetic grids.

The density separation process can be described with the aid of the apparent density profile shown in Figure 7. This is a plot of the apparent density, on the vertical plane midway between a pair of poles or wires, versus the height above the grid. The shape of the curve can be determined from the function f_n of Figure 5. The maximum apparent density occurs at the critical point and is termed the critical density ρ_c. A heavy object of density $\rho_H > \rho_c$ will not intersect the apparent density curve for any values of the altitude z. Such an object will sink and pass through the grid. The line representing the density of a light object $\rho_L < \rho_c$ will intersect the apparent density curve twice. The upper intersection is a point of stable equilibrium but the lower point is unstable. The object cannot rest here but must sink or float. In fact, there are no positions of stable equilibrium below the critical point for objects denser than ρ_f. This is significant because it means that objects cannot clog the grid.

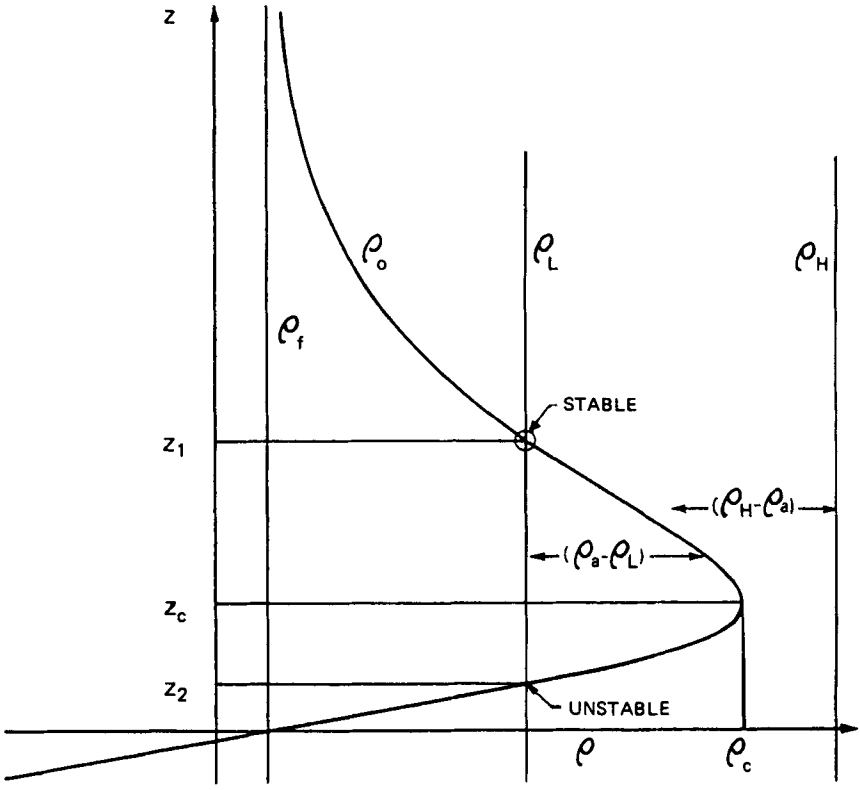

FIGURE 7 The apparent density profile. Intersections of constant density lines yield stable equilibrium points above the critical point and unstable equilibrium points below the critical point.

Above the critical point objects of density between ρ_f and ρ_c will float at a level where their density equals ρ_a. While it is possible to consider collecting particles at different heights to obtain a fractionation according to density, it is more practical to use the grid as a binary separator. In operation, particles are fed to the grid near but above the height of the critical points. Particles less dense than ρ_c

will float above the grid where they can be removed laterally. The vertical components of initial kinetic energy of the particles must be kept small so that the particles cannot puncture the barrier. Particles more dense than ρ_c will sink through the grid where they can be collected and removed.

It has been assumed that the grid is horizontal. Tilting of the grid plane can be beneficial because it permits using some of the gravitational force to transport material over the grid. It is convenient to rotate the coordinate frame with the grid and then determine the forces normal to and perpendicular to the grid. The vertical component of the gradient, Figure 6, is now the normal component. The gravitational force may be decomposed into tangential and normal (to the grid) components by replacing $\vec{g}$ in Eq 1 with g sinα and -g cosα, where g is the scalar acceleration of gravity and α is the angle of tilt of the grid normal from the true vertical. For a tilted grid, there is no true equilibrium; the tangential component of the force is always finite for all values of particle density $\rho_o > \rho_f$. The normal component of the force is zero when

$$(\rho_a - \rho_f) = (\rho_o - \rho_f) \cos\alpha \tag{9}$$

The value of ρ_o that satisfies Eq 9 can be considered to be the critical density ρ_c for a tilted grid when ρ_a is equal to the critical density ρ_{co} for a horizontal grid. Eq 9 may be written

$$(\rho_{co} - \rho_f) = (\rho_c - \rho_f) \cos\alpha \tag{10}$$

The critical density for a tilted grid may thus be readily calculated from that of a horizontal grid. Note that ρ_c is larger than ρ_{co}, which means that denser objects may be floated on a tilted grid. This does not mean that the vertical force is larger; it is actually less than that of a horizontal grid. The particles are not in equilibrium but are accelerated downward along the inclined plane of the grid.

Design of Multiple-Gap Magnetic Grids

The magnetic grids described so far are idealized structures. The problem of building real structures that approximate the ideal will now be considered.

It is possible to construct a grid of current-carrying wire, rod or tubing that goes back and forth in a plane in a shape similar to the grids of early vacuum tubes. Such a grid would be a direct analog of the grid wires used in the Ampere's-law method of calculating the fields. It is usually more practical to make grids of magnetic poles, rather than current-carrying wires, and only permanent-magnet grids will be described in detail.

The magnetic grid is an alternating array of N and S parallel, cylindrical magnetic poles in a plane. The poles can be simple cylinders of iron. The simplest way to create and maintain the field is to place ferrite permanent magnets between the bars. Since the grid must have open gaps these magnets are placed at the ends of the rods. Such grids are multilayer "sandwiches" of iron and ferrite. This forces the ferrite to be the same thickness as the gap. This would be a detriment with an alloy magnet, due to the large demagnetizing field, but ferrite magnets can be sufficiently hard to be uneffected. The magnet cross-sectional area must be large enough to supply the needed flux. This means that the poles must be enlarged to form a pad to contact the magnet area. It is desirable to smoothly join the gap and pad regions through a concentrator section. Finally, in order to keep the top surface in a single plane, all depth changes are made on the bottom side of the grid. The elevation profiles of such grids assume a general shape that we call a "hunched beam" or "half-dog-bone." Examples of such grid profiles are shown in Figure 8.

Several methods have been used to design the proportions of the grids. Various grades of ferrite are available (Grades 1-8) depending on the material and its flux density. Grade 1 is weak and requires a larger pad area than Grade 6 or 7 to produce the

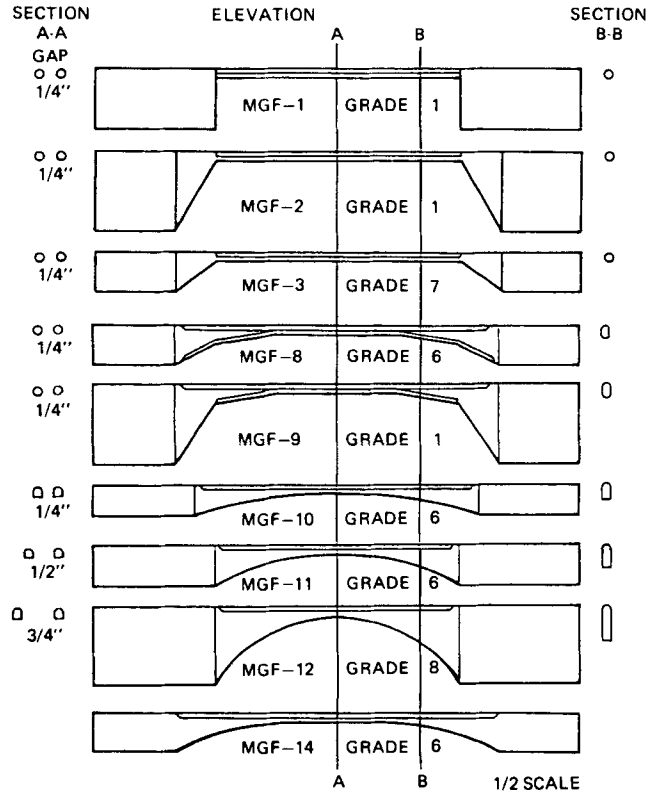

FIGURE 8 Magnetic grid filter designs.

same flux. The design procedure depends on estimating the permeance of the iron circuit. Since the grid is a repetitive structure, only a single section need be calculated. The permeance of the section is computed using standard formulas for the different shaped regions of the bars. As in most magnet design, the biggest uncertainties come in estimating the leakage and reluctance corrections.

The design is also complicated by the fact that the grid will be used immersed in ferrofluid. This magnetizable medium acts as an additional load on the grid. This load alters the magnetic properties of a dry grid. This effect may be illustrated by

examining the second quadrant demagnetizing curve for the ferrite as shown in Figure 9. Demagnetizing curves for several grades of ferrite are shown. The operating point will be determined by the intersection of a load line with the curve. The slope of the load line is $-\lambda$, where λ is the "unit permeance" or total permeance times the magnet length divided by the magnet area. For a dry grid, this load line passes through the origin. In ferrofluid, the load line is altered in a complex manner. However, if the ferrofluid is assumed to be saturated at I_s, then it may be shown that the load

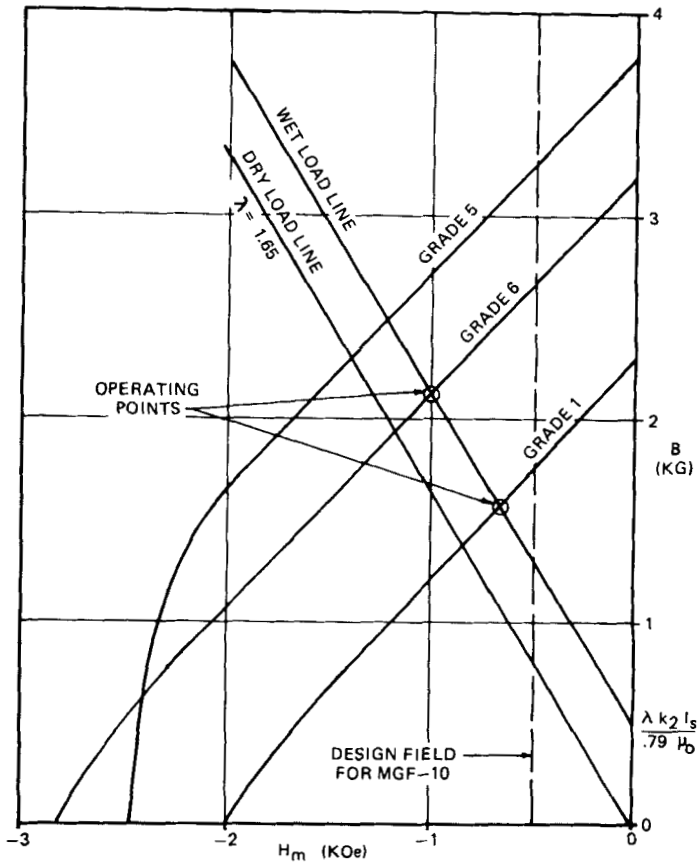

FIGURE 9 Demagnetization curves, load lines and operating points for ferrite driven magnetic grid filters.

line is changed to

$$B = -\lambda \left[H_m - k_2 I_s/.79\mu_o \right] \quad (11)$$

where k_2 is a reluctance correction factor somewhat greater than unity and μ_o is the permeability of space. The effect of the fluid is to shift the load line to the wet load line shown in Figure 9.

An illustration of a completed and assembled magnetic grid structure is shown in Figure 10. Note that the grid can be extended laterally to any distance by adding sections. Various means, other than the bolts shown in Figure 10, may be used to hold the assembly together.

Characteristics of Magnetic Grid Filters

Some, but not all, of the grids designed and shown in Figure 8 have been built and tested. Although the grid will be used in ferrofluid, the simplest tests involve measurements of the magnetic field in the gaps of a dry grid with a Hall probe. For example, a probe made to detect and measure the fluid strength of lateral flux lines was rigidly mounted in a fixed position. The grid to be tested was mounted on a table that could be accurately translated

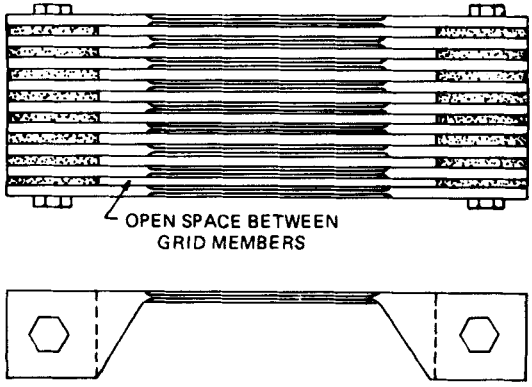

FIGURE 10 Drawing of assembled magnetic grid.

vertically and horizontally with lead screws. By adjusting the screws, the field could be probed longitudinally along the gaps or vertically up through the gaps. The middle of the central gap (for an even number of bars) was taken as the origin.

The measured longitudinal variation of the central field for an early grid (MGF-2) is shown in Figure 11. Data were taken for a two-bar grid (single gap) and a four-bar grid (three gaps). The additional bars lower the field intensely because they are of opposite polarity and oppose the field from the original pair of bars. The longitudinal variation of the field is rather slight, until the concentrator region is reached. Later measurements have shown that some grid designs have greater longitudinal variation.

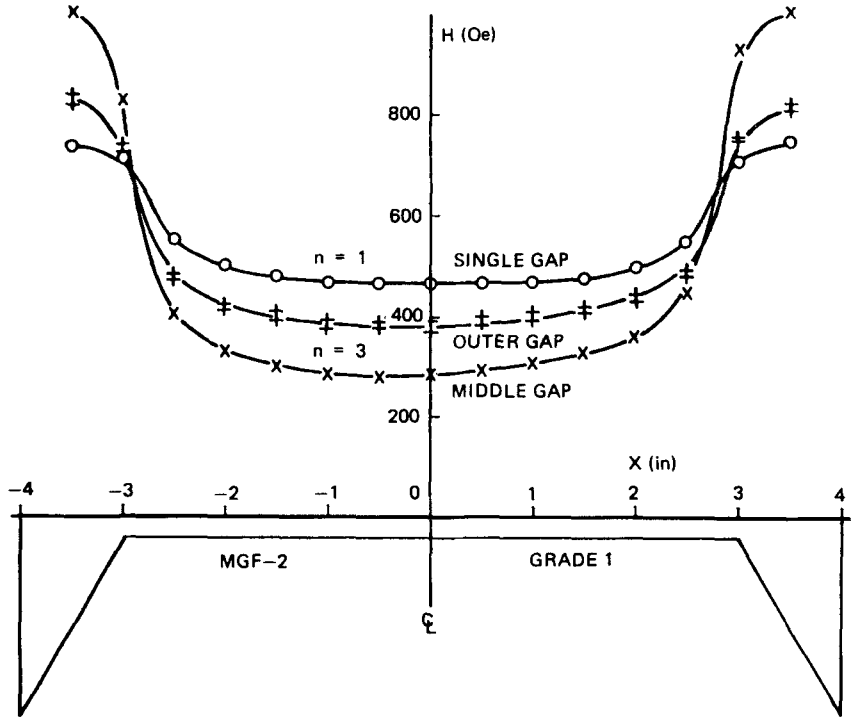

FIGURE 11 Measured longitudinal variation of field strength for 2-bar and 4-bar arrays.

The theoretical assumption that the grid bar is a surface of constant magnetomotive force cannot hold in reality for bars where the gap width is constant. The field will always be lowest in the center and somewhat higher near the ends. This does not prevent accurate density separation since the light fraction flows over the grid surface and passes the central region. The critical density is determined by this region.

The measured vertical variation in the field strength, relative to the standard central field, is shown in Figure 12. Data are presented for 1, 3, 5, 7 and 9 gaps. The curves are quite similar in shape to the theoretical function h_n in Figure 4. The curves oscillate as n increases but quickly converge to a curve somewhat below the theoretical estimate. Even the predicted

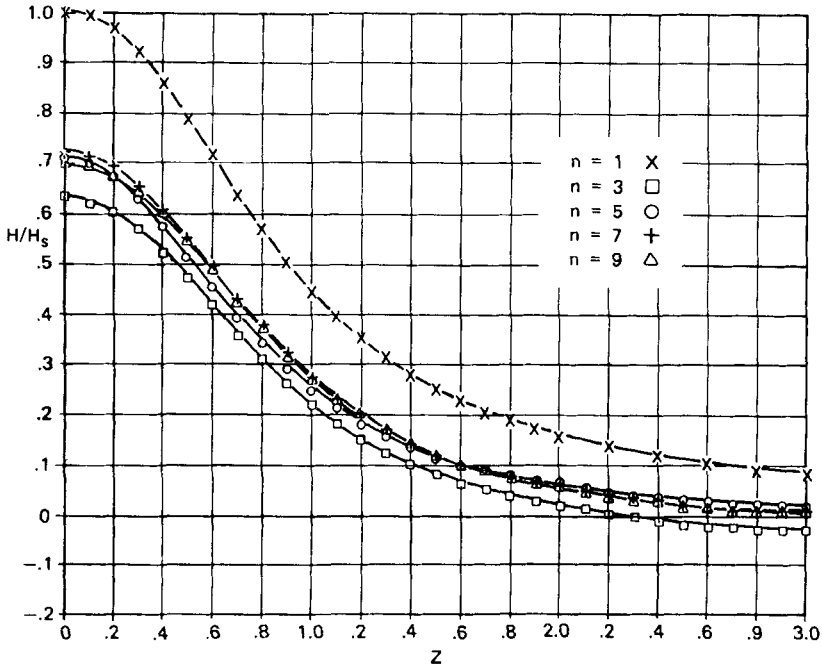

FIGURE 12 Measured vertical field profiles for arrays with odd number of gaps n. Compare with the calculated function h_n in Figure 4.

negative values are observed at high levels above the three-gap grid. The field gradients ∇H_z have been determined from the same data. The values were normalized by computing $b\nabla H_z/4\ H_s$, where b is the gap-to-gap dimension of the grid, and are plotted in Figure 13. These curves can be compared with the function f_n in Figure 5. The measured single gap peak value is somewhat high, possibly because the poles were not round but were chamfered

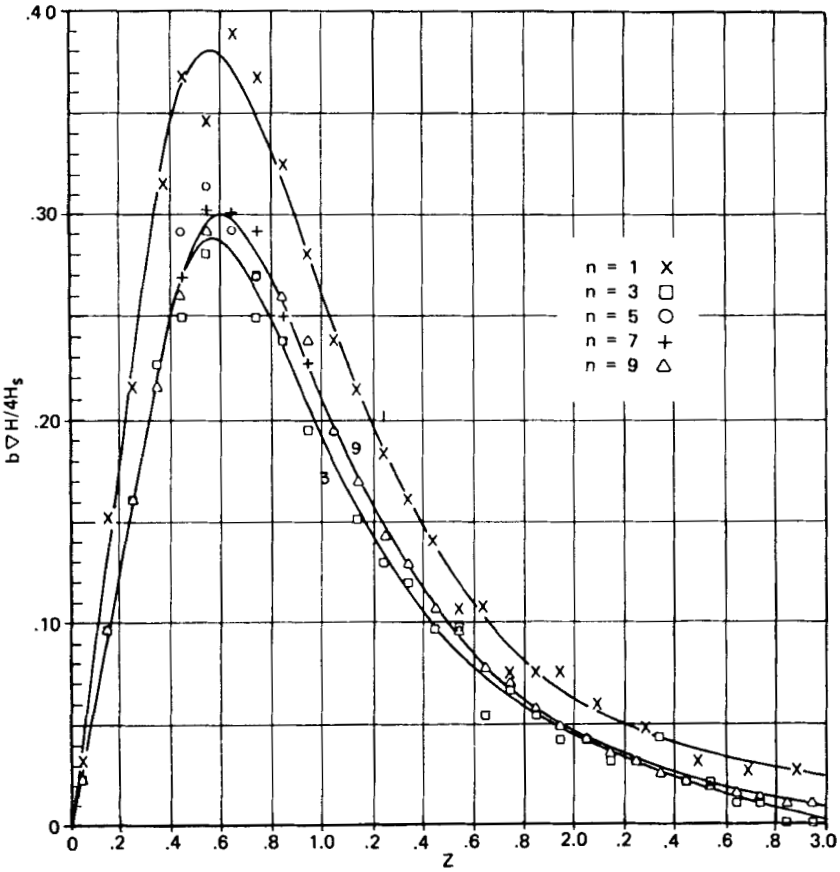

FIGURE 13 Measured vertical gradient profiles for arrays with odd number of gaps n. Compare with the calculated function f_n in Figure 5.

square sections. Note however, that the peak approaches 0.3 for higher number of gaps, in excellent agreement with the theory.

A similar procedure has been used to measure the vertical profiles in each gap of a 10-bar, 9-gap array. The values of the peak field and peak gradient are presented in Figure 14. The field intensity is noticeably high in the outer gaps and low in the next-to-outer gaps. The measured values of the peak gradient show rather little variation about the mean value of 0.31. These data

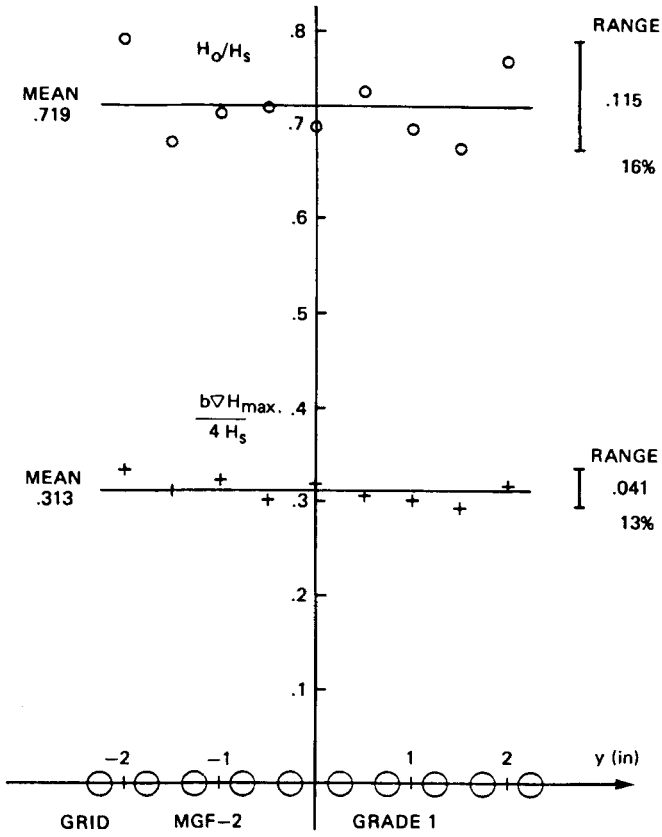

FIGURE 14 Measured central fields and peak gradients for each gap of a 10-bar array.

indicate that the theory of ideal grids may be applied to real grids with confidence. The observed properties and variations of properties of real grids agree well with the predictions.

The behavior of a magnetic grid in a density separation depends on the strength of the ferrofluid as well as the strength of the ferrite and the permenace of the grid structure. The linear portion of the demagnetization curve for the ferrite may be expressed as

$$B_m = B_r + \mu_r H_m \tag{12}$$

where the recoil remanence μ_r only slightly exceeds the permeability of space μ_o. As stated above, the operating point is the intersection of the demagnetizing curve with the wet load line, Eq 11. The magnet field, $(-H_m) = k_2 H_g$, is related to the standard central field, and this field, $H_s = 0.81\, b\nabla H_c$, is related to the magnet period and the critical gradient. The gradient is related by Eq 3 or Eq 4 to the critical apparent density, and by Eq 10 to the tilt angle. The net result of combining these relationships is a characteristic equation for the grid of the form

$$(\rho_c - \rho_f)\cos\alpha = \frac{K I_s (B_r - k\lambda I_s)}{(\mu_r + \lambda) b} \tag{13}$$

where K and k are constants, I_s is the saturation magnetization of the ferrofluid, B_r is the remanent magnetization of the ferrite, μ_r is the recoil remanence, λ is the unit permeance, and b is the period or gap-to-gap spacing.

The values of the constants K and k depend on the units employed. Numerical values have been determined but so many assumptions have been used in the derivation that it is preferable to consider these as empirical parameters to be determined by experiment.

The form of the characteristic curves calculated by Eq 13 is shown in Figure 15. The remanent magnetization has been taken to be 3200 G, the value for a Grade 6 ferrite, and the grid period is 1/2-inch. The density is expressed in specific gravity units and the fluid strength in gausses. Curves are shown for various

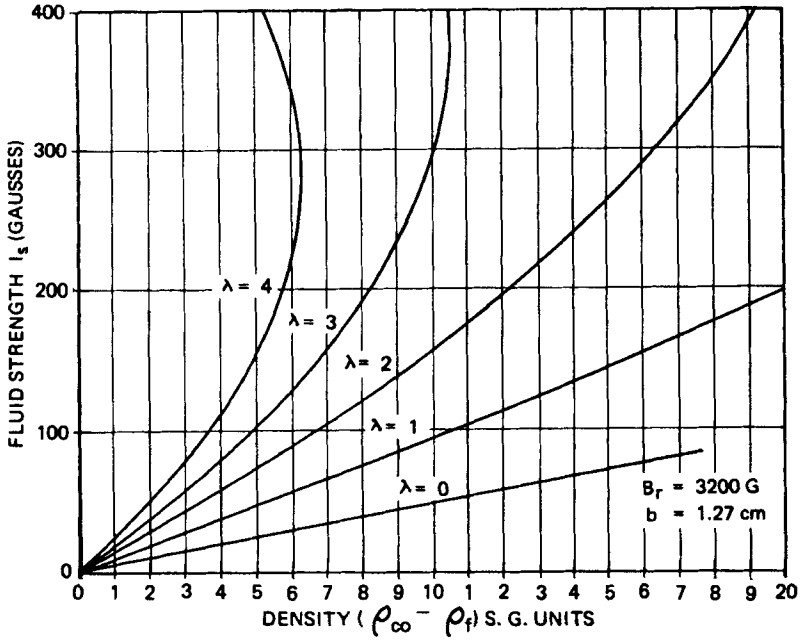

FIGURE 15 Characteristic curves for various values of unit permeance. The curves were computed from Eq 13 using B_r = 3200 G and b = 1.27 cm. Note the negative slopes possible for high fluid strength and high unit permeances.

values of the unit permeance λ. For low values of λ, the critical density increases as the fluid strength increases. For high values of λ, there is a maximum critical density and the apparent density decreases with further increases in fluid strength. This is because the fluid loads the magnetic circuit. The maximum in apparent density has been observed in experimental tests with strong fluids and high-permeance grid structures.

A few experiments have been made to directly measure the buoyant forces on a small object in the gap of a magnetic grid immersed in ferrofluid. The object was a small tungsten cylinder connected by a thin rod to an analytical balance. These tests proved that an object is laterally stable on the central plane of

the gap and confirmed the general form of the apparent density profile, Figure 7, for positions above the critical point. A balance of forces could not be achieved below the critical point proving that this region is unstable as predicted. The resulting apparent density profile is shown in Figure 16 by the solid line. The dashed line indicates the region where a balance of forces could not be achieved. In these tests, the magnetic grid was assembled with ferrite magnets with a measured B_R=2600G, and the fluid's intensity of magnetization was measured at 280 gausses.

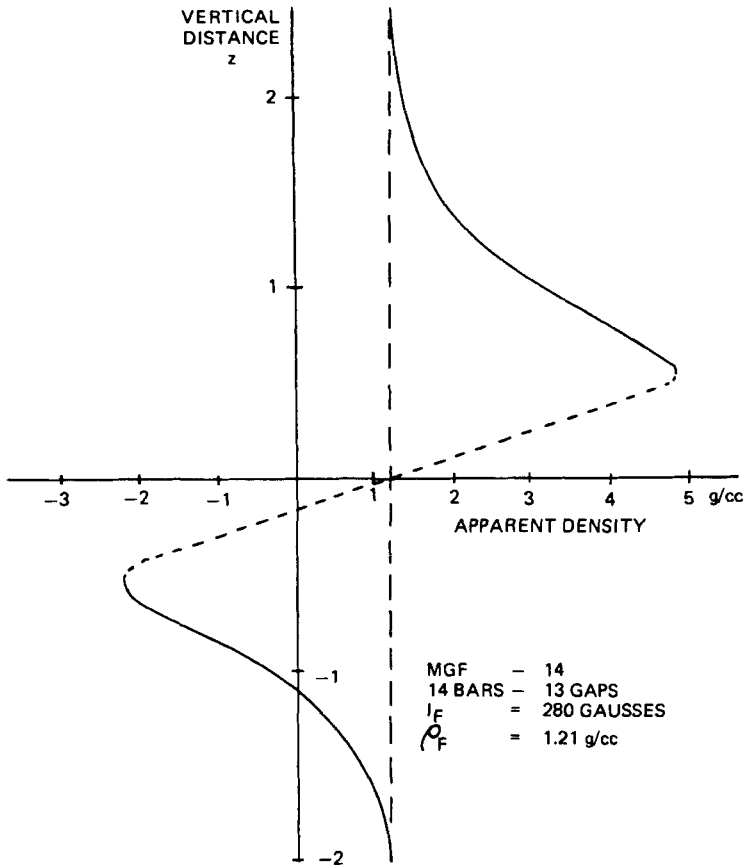

FIGURE 16 Density profile for a magnetic grid in ferrofluid.

Density Separations with Magnetic Grid Filters

A laboratory separator was designed specifically for the experimental study of density separations with the magnetic grid filter. It consisted essentially of a box in which the magnetic grid and the ferrofluid were contained, a means of introducing the material to be separated in the vicinity of the magnetic grid, and two removable containers to receive the separated fractions. The grid plane could easily be tilted by rotating the small laboratory separator through the desired angle.

Density separations were conducted using mixtures of sand (ρ = 2.6 g/cc) and zirconia (ρ = 5.6 g/cc). The particle size was varied from 2.0 mm down to 74 microns. Several different mixtures were used. The mixtures to be separated contain 40, 10 and 1 percent by weight of zirconia.

Separation of mixtures containing large particles, 2.0 or 0.5 mm, with 40 percent by weight will be described first. Figure 17 shows the effect of the intensity of magnetization or fluid "strength", and of the grid tilt angle, on the composition of the sink fraction in weight percent of zirconia. For binary separation, the fluid strength has little influence above a critical value. For weaker fluids, the apparent density rapidly approaches the density of sand and allows sand particles to pass through the grid. For coarse particles, the tilt angle does not seem to have much influence.

As the particle size is decreased, the separation follows a more complex behavior. As the tilt angle increases, the quality of the separation seems to be adversely affected. Small particles seem to be entrained by their neighboring particles and end up in the wrong direction: some zirconia particles over the surface of the grid with the majority of the sand particles, and some sand particles through the grid with the majority of the zirconia particles. This behavior seems to result from the hydrodynamics and surface chemistry of the fine particles in the fluid.

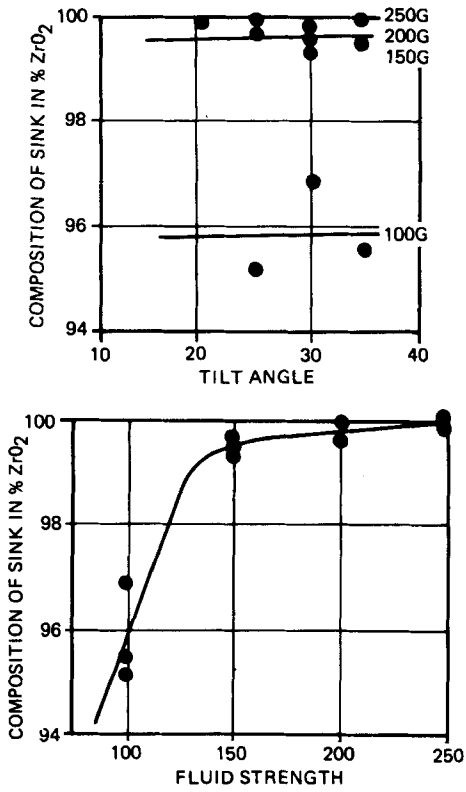

FIGURE 17 Effect of fluid strength and tilt angle on the sink fraction for a 40% zirconia - 60% sand mixture. Particle size: 2.0 to 0.5 mm.

Figure 18 shows the results of separations obtained from mixtures of fine particles, 250 to 74 microns, containing only 1 percent by weight of zirconia. The amount of zirconia in the sink fraction now depends on the grid tilt angle. Small tilt angles yield better separation. The effect of fluid strength indicates that intermediate fluid strengths are preferred, specially at small tilt angles.

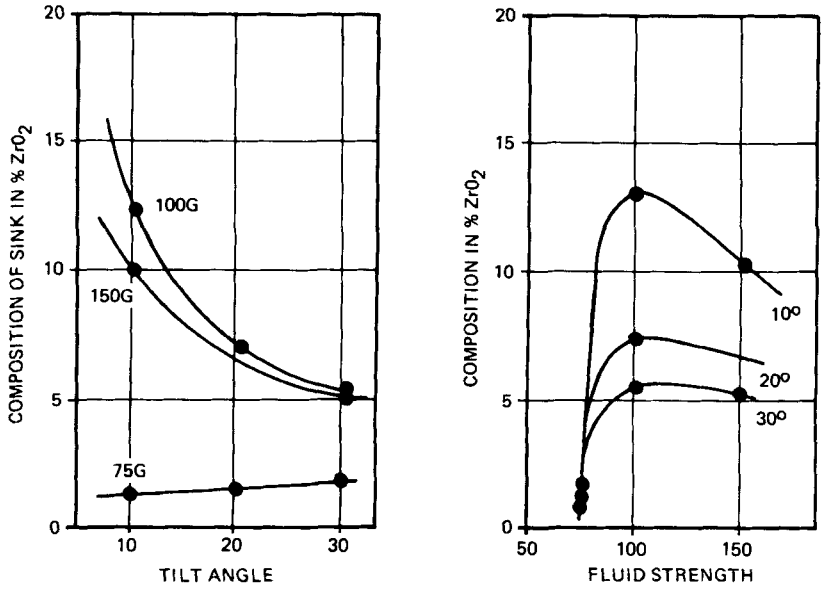

FIGURE 18 Effect of fluid strength and tilt angle on the sink fraction for a 1% zirconia - 99% sand mixture. Particle size: 250 to 74 microns.

Separation made with mixtures containing various amounts of zirconia, 40, 10 and 1 percent by weight, can also be used to demonstrate an important feature of the magnetic grid filters. Consider a mixture of fine zirconia and sand particles (250 to 74 micron in size) containing only 1 percent by weight of zirconia. Zirconia is to be recovered from this mixture by density separation. For the process to be efficient, the sink fraction must contain a high percentage of zirconia and little sand, and most of the zirconia should be recovered.

Examination of Figure 18 reveals that the separation of 1 percent zirconia mixture with 100 gauss fluid strength and a 10 degree tilt angle will yield a sink fraction containing 13 percent zirconia. This sink fraction can be separated again to yield a sink fraction of higher zirconia content and a second float fraction. This operation can be repeated as many times as

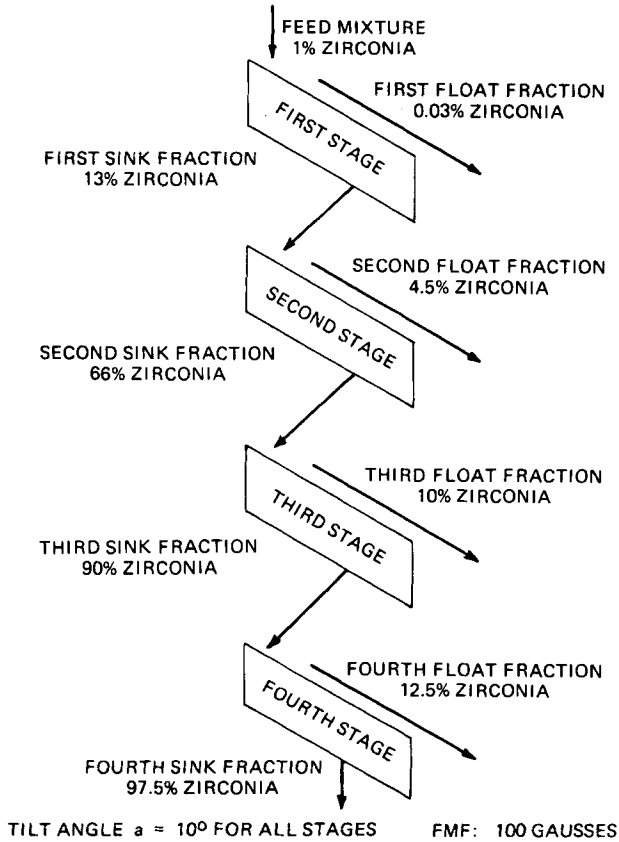

FIGURE 19 Schematic diagram of four magnetic grids assembled in a multistage system.

needed to obtain a final sink fraction containing the desired concentration of zirconia. Similarly, each resulting float fraction can be processed again to recover its zirconia content.

For a practical system capable of performing multiple separation, several magnetic grid filters can be stacked on top of each other, and aligned end-to-end in a "multistage" separator, each stage performing one specific separation. From these and other experimental measurements we can calculate that, for a mixture containing 1 percent zirconia, a stack of four grids

would yield a final concentrated sink fraction containing 97.5 percent by weight zirconia, Figure 19. The first float fraction contains only 0.03 percent by weight zirconia, and can be arbitrarily discarded. All other float fractions contain too much zirconia to be discarded. They can all be further treated and returned to an upper stage, either individually or combined. An alternative for treating the float fractions again, is to extend each stage with one or several grids end-to-end. A vertical and lateral magnetic grid can be assembled in this fashion, to develop a multistage system engineered to obtain the maximum efficiency for a specific separation.

CONCLUSION

Magnetic grids consist of planar arrays of parallel bars of alternating polarity driven by permanent magnets. Magnetic grids can be designed by considering ideal grids. They can be constructed from shaped iron bars and commercial ferrite magnets. Magnetic measurements qualitatively agree with the theoretical predictions derived from the study of ideal grids.

Magnetic grids submerged in ferrofluid have demonstrated the capability to perform binary separations of mixtures of particles of different densities.

Assembled in a multistage system, magnetic grids are capable of efficient density separation of mixtures covering a wide range in size, including fine particles in the micron range.

ACKNOWLEDGEMENTS

This work was performed when the authors were members of the Union Carbide Corporate Research Laboratory, Tarrytown, NY 10591.

The authors express their appreciation for the assistance and cooperation of Drs. H. Hatwell and P. Leung and Messrs. A. Paulsen and J. Farkas.

REFERENCES

(1) B. Berkovsky and R. E. Rosensweig, J. Fluid Mech. 87 (3), 521 (1978)

(2) R. E. Rosensweig, Int. Sci. Technol. 55, 48 (1966)

(3) R. E. Rosensweig, Nature 210, 613 (1966)

(4) R. E. Rosensweig, U. S. Patents 3,483,969 (Dec. 1969) and 3,488,531 (Jan. 1970)

(5) R. Kaiser, U. S. Patent 3,483,968 (Dec. 1969)

(6) S. E. Khalafalla and G. W. Reimers, Sep. Sci. 8 (2), 161 (1973)

(7) G. W. Reimers, S. A. Rholl and S. E. Khalafalla, U. S. Patent 3,788,465 (Jan. 1974)

(8) Avco Corporation, NASA Contract NAS 1-11793 (June 1973)

(9) G. W. Reimers and S. E. Khalafalla, U. S. Patent 3,843,540 (Oct. 1974)

(10) The intensity of magnetization I is related to the induction B and field H by $I = B - \mu_o H$ where μ_o is the permeability of space. The derivations and analyses conform to S.I. units where I is in teslas (T), H in ampere turns per meter (A/m) and μ_o is $4\pi \times 10^{-7}$ henry/m. I and B may also be expressed in gausses (G), where 10^4 G is equivalent to 1 T, and H in oersteds (Oe) where 1 Oe is equivalent to 79.6 A/m. In the gauss-oersted system μ_o is unity.

(11) H. Fay, Rev. Sci. Instrum. 43, 1274 (1972)